**ICMIEE22-134**

# Electrothermal Analysis of Graphite-Reinforced Metal Matrix Composites for High-Temperature Resistive Heating Applications

*Asif Faisal Beg*, Fahim Khan, S Reaz Ahmed*
Department of Mechanical Engineering,
Bangladesh University of Engineering & Technology, Dhaka 1000, Bangladesh

**ABSTRACT**

Resistive heating capability of a graphite-reinforced metal-matrix composite (MMC) is investigated through the corresponding electrothermal responses under a DC field. The steady-state electrothermal behavior of the MMC is analyzed using a direct computational scheme under forced convection air cooling. Tungsten matrix reinforced by graphite fibers is considered as the MMC for its higher melting and operating temperature along with high strength characteristics. The governing partial differential equations are modified to be compatible with solving the multi-domain thermal problem coupled with the electrical problem of composite materials. An efficient iterative scheme is developed to couple the electrical problem with the multi-domain thermal problem. The effect of electrical heating is then post-processed by evaluating the temperature of the working fluid at the exit of the resistive heating unit. The effect of fiber volume fraction and orientation of the graphite fibers in the MMCs is also investigated under similar conditions. It has been observed that the resistive heating capability of the present MMC systems is better than the conventional material, *Nichrome*. Moreover, the resistive heating ability of the MMC increases significantly at higher volume fractions of graphite in both the fiber orientations, although the rising trends are different.

Keywords: Electrothermal analysis, metal-matrix composite, resistive heating, computational iterative scheme

## 1. Introduction

For years, Nickel-based and Iron-based alloys have been used as heating elements in electric heating applications [1]. Among these alloys, *Nichrome* (80% *Ni* - 20% *Cr*) is currently the most used [2]. *Nichrome* is cheap, available, and has a high melting point, high tensile strength, and high resistivity. However, there are even cheaper alloys like Kanthal *FeCrAl* alloy (20%-30% *Cr*, 4%-7.5% *Al*). Kanthal also has better tensile and resistive properties [3]. Both these alloys have a melting point of around 1400-1500℃, restricting their service ceiling to around 1200-1300℃. Even a higher service ceiling can be achieved by using $MoSi_2$ [4] and *SiC* [5]. These materials can continue heating up to 1600-1800℃. Composite materials are increasingly breaking into structural applications and a range of other uses due to the enhanced special qualities and the ease with which these properties may be regulated during production. Several types of composites are very popular and in operation in today's markets. Among them, Polymer matrix composites (PMC), Metal matrix composites (MMC) and Ceramic matrix composites (CMC) are the most common. Metal matrix composites provide various advantages like higher stiffness, higher strength, high operating temperature, tunable thermal conductivity, and tunable electrical conductivity. The use of MMC in structural applications is indispensable [6]. MMCs are also stepping into thermo-mechanical applications in rapid succession [7]. Graphite fibers provide advantages like a low coefficient of thermal expansion, comparatively higher resistivity and higher strength [8]. Refractory carbide-reinforced tungsten composites are the most recent inclusion in this field. High microstructural stability and high temperature mechanical, thermo-physical and chemical properties made them promising candidates in industrial, military and aerospace sectors [9].

In the present research, the potential of graphite-reinforced MMC as the resistive heating element is analyzed in terms of the corresponding electrothermal characteristics under a DC field with the influence of local forced convection air cooling. The results are then compared with those of traditional resistive heating alloys. The resistive heating capabilities of both composite and alloy are analyzed over a wide range of input conditions. Also, the effects of fiber volume fraction and fiber orientation on resistive heating capabilities are quantified. Finally, the use of MMC and its effect on electrical heating efficiencies are also analyzed and discussed.

## 2. Electrical and thermal properties of MMCs

Composites are transversely isotropic materials with different magnitudes of the property parallel to the axis of fibers (longitudinal) and perpendicular to the fibers (transverse) axis. The mathematical models to determine the thermal and longitudinal electrical properties of metal matrix composites (MMC) are very similar to those of polymer matrix composites (PMC) and are widely available. The electrical resistivity of MMC in the longitudinal direction for a composite consisting of homogenous tungsten fibers is given by David L. McDanels [10]

$$\frac{1}{\rho_l} = \frac{V_f}{\rho_f} + \frac{V_m}{\rho_m} \tag{1}$$

* Corresponding author. Tel.: +88-01521419934
E-mail addresses: mdfaisalbegasif@gmail.com

Where, $\rho_l$ , $\rho_f$ & $\rho_m$ are electrical resistivity of composite in longitudinal orientation, fiber and matrix materials respectively. And $V_m$ $and$ $V_f$ represent matrix and fiber volume fractions. He also predicted the thermal conductivity in the longitudinal orientation to be,

$$k_l = k_f V_f + k_m V_m \tag{2}$$

With $k_l$ , $k_f$ & $k_m$ to be the thermal conductivity of composite in longitudinal orientation, fiber and matrix materials, respectively. The same Eq. (2) is stated by Barbero [11] afterward. The thermal conductivity in the transverse direction can be given as,

$$\frac{1}{k_t} = \frac{V_f}{k_f} + \frac{V_m}{k_m} \tag{3}$$

However, Eq.(3), developed by the rule of mixtures, gives the lower limit value of the transverse thermal conductivity. The upper limit value can be given as [12],

$$k_t = Bk_m V_m + \frac{V_f + (1-B)V_m k_f k_m}{V_f k_m + (1-B)V_m k_f} \tag{4}$$

There are rarely direct models available to determine the transverse electrical properties of PMCs, as the associated conduction of current in the transverse direction is negligible. There are eddy current [13] and several other methods to determine such low conductivity. However, unlike PMCs, the matrix material in MMC is also a good conductor of current, invalidating the negligibility of current flowing along the transverse direction. In this work, a simplified model is formulated to determine the transverse electrical resistivity, which is

$$\rho_l = \rho_f V_f + \rho_m V_m \tag{5}$$

Later, this formula was verified using the mixture law in a fashion similar to that used in transverse thermal conductivity.

## 3. Problem statement

The resistive heating capabilities of thin Tungsten matrix with reinforcing graphite fiber *(W-C)* plates of two different orientations and that of identical *Nichrome (Ni-Cr)* plate are analyzed. Air under forced convection is used as the working fluid. Air is flown over the electrically heated plate setups to dissipate the heat. The temperature rise of air leaving the setup is measured and used as an indicator of the resistive heating performances of the heating elements.

The schematic diagram of the composite plates with length $L_x$, width $L_y$ and thickness $t$ (=100μm) is illustrated in Fig.1. Later in this paper, Tungsten-graphite composite with longitudinal fiber orientation and transverse fiber orientations are denoted as *W-C(l)* and *W-C(t)* respectively.

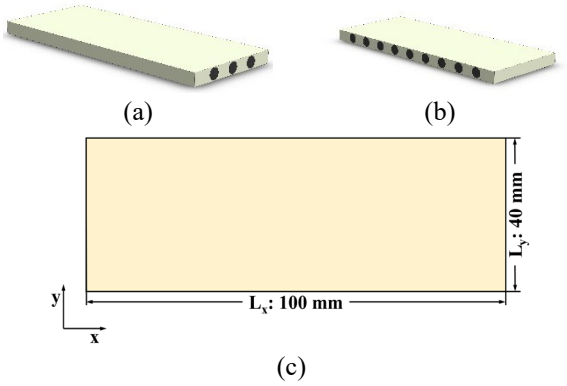


**Fig.1** Tungsten-graphite composite with (a) longitudinal and (b) transverse fiber orientation. (c) dimension of the composite plates.

3.1 Experimental setup

The schematic diagram of the experimental setup followed in this investigation is illustrated in Fig.2.

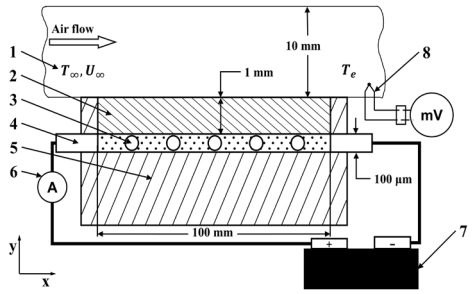


**Fig.2** Schematic drawing of the resistive heating unit assembly

In the setup, the air is forced into the resistive heating unit with a velocity of 10 m/s from the left side of the setup along to the positive x direction. The inlet temperature and thickness of air are maintained at 300 K and 10 mm. At the right end of the setup, a set of thermocouples are placed to record the exit temperature of hot air. The differences in exit and inlet temperature are then calculated and used as a measurement of resistive heating capacity. The heating unit consists of an Insulating body that provides both electrical and thermal insulation from the environment and structural support. An identical secondary layer of thickness 1mm of material *BeO* is used on top of the electrical heating element. The high electric insulating property *BeO* helps avoid any electric contact between the electrical heating element and working fluid to ensure the unit's compatibility to use water or lubricating oils as working fluid. *BeO* also has very high thermal conductivity, ensuring homogeneous and improved heat transfer between air and the heating element. The electrical heating element has two current Input/Output pads

connected on both ends along the length. Current ranging from 4 to 320A (0.1 x$10^7$-8 x$10^7$ A/m$^2$) is supplied via the pads with the help of a DC power supply. The direction of the current flow is kept from left to right along the length of the element for all instances.

3.2 Material properties

The individual material properties of the *Tungsten* matrix, *graphite* fiber, *Nichrome* and *Beryllium oxide* are given in Table 1 [14].

**Table 1** Thermoelectrical properties of materials

| Material Name | Electrical resistivity (Ω m) | Thermal conductivity (W/m K) | Melting point (°C) |
|---|---|---|---|
| *Tungsten* | 1.12e-7 | 170 | 3422 |
| *Graphite* | 8e-6 | 1600 | 3600 |
| *Nichrome* | 1.12e-6 | 11.3 | 1400 |
| *BeO* | - | 285 | 2500 |

The material properties for *W-C(l)* and *W-C(t)* are determined using Eq. (1), Eq. (2), Eq. (3) and Eq. (5) for respective fiber volume fractions.

3.3 Failure criteria

The melting failure of the electrical heating element is used as the main failure criterion in this experiment. The melting point of the tungsten matrix and graphite fiber in composites is way over 3000°C. However, by taking the structural stability into account, the maximum operating temperature of composite heating elements is kept around 2400K. This consideration also prevents the possibility of melting failure of the secondary layer with a melting point of around 2500°C. A maximum operating temperature of around 1400K is used in the case of the *Nichrome* heating element.

## 4. Mathematical background

4.1 Electrical problem

The two-dimensional form of the governing equation of electric field for composite materials,

$$\frac{1}{\rho_l}\left(\frac{\partial^2\varphi}{\partial x^2}\right)+\frac{1}{\rho_t}\left(\frac{\partial^2\varphi}{\partial y^2}\right)=0 \tag{6}$$

In Eq. (6) the $\rho_l$ and $\rho_t$ denotes the longitudinal and transverse electrical resistivity of composite materials. However, for isotropic materials like pure materials and alloys, both the directional properties become equal.

4.2 Thermal problem

The steady-state governing differential equation of the temperature field of a thin metal plate can be expressed as,

$$\frac{\partial}{\partial x}\left(k_l\frac{\partial T}{\partial x}\right)+\frac{\partial}{\partial y}\left(k_t\frac{\partial T}{\partial y}\right)-H+G=0 \tag{7}$$

Here, T is the value of the temperature field at any point, $k_l$ and $k_t$ are the longitudinal and transverse thermal conductivity of composite materials, $G$ is heat addition, and $H$ denotes heat dissipation. For isotropic materials, $k_l = k_t = k$. The joule heat generation by the electric field is expressed by,

$$G=\frac{1}{\rho_l}\left(\frac{\partial\varphi}{\partial x}\right)^2+\frac{1}{\rho_t}\left(\frac{\partial\varphi}{\partial y}\right)^2 \tag{8}$$

However, this resistive heating unit consists of more than one domain where the temperature field is solved. In the primary heating element, heat is generated by joule heating and dissipated by the secondary layer from the top surface. So, the governing equation for the primary heating element is,

$$k_l\frac{\partial^2T_1}{\partial x^2}+k_t\frac{\partial^2T_1}{\partial y^2}+\frac{1}{\rho_l}\left(\frac{\partial\varphi}{\partial x}\right)^2+\frac{1}{\rho_t}\left(\frac{\partial\varphi}{\partial y}\right)^2+\frac{2K_{C1}}{(t_1+t_2)}\frac{T_2-T_1}{t_1}=0 \tag{9}$$

Here, $T_1$, $T_2$, $t_1$ *and* $t_2$ are the temperature and thicknesses of the electrical heating element and secondary layer, respectively. $K_{C1}$ denotes the equivalent thermal conductivity of heat transfer between two layers along the z direction. Similarly, the governing equation for the secondary layer can be written as,

$$k_2\frac{\partial^2T_2}{\partial x^2}+k_2\frac{\partial^2T_2}{\partial y^2}-\frac{2K_{C1}}{(t_1+t_2)}\frac{T_2-T_1}{t_2}-h\frac{T_2-T_a}{t_2}=0 \tag{10}$$

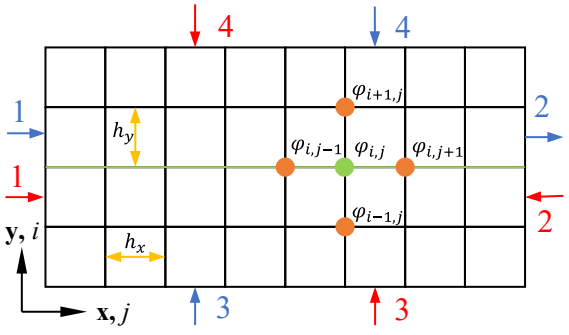


Electrical problem

1. $\frac{\partial\varphi}{\partial x}=-\rho_x J$
2. $\frac{\partial\varphi}{\partial x}=-\rho_x J$
3. $\frac{\partial\varphi}{\partial y}=0$
4. $\frac{\partial\varphi}{\partial y}=0$

Thermal problems

1. $\frac{\partial T}{\partial x}=0$
2. $\frac{\partial T}{\partial x}=0$
3. $\frac{\partial T}{\partial y}=0$
4. $\frac{\partial T}{\partial y}=0$

**Fig.3** Boundary conditions and sample mesh diagram of the electrothermal problem

In Eq. (10), $h$ is the local convection heat transfer coefficient and $T_a$ is the temperature of air. The temperature of the air domain is determined using,

$$hA_s(T_2 - T_a) = \dot{m}C_p\Delta T_a \quad (11)$$

Here, $A_s$ , $T_a$, $\dot{m}$ and $C_p$ are surface area exposed to airflow, temperature, mass flow rate and specific heat capacity of air, respectively.

Fig.3 shows the boundary conditions for the electrothermal problems where 1 and 2 indicate the entrance and exit of current density $J$ for the electrical problem. The rest of the boundaries are kept electrically insulated. And for all the thermal domains, the thermal insulation boundary condition is applied.

## 5. Numerical modeling and solution

The corresponding governing differential equations are solved computationally using the Finite difference (FD) technique. A uniform high-density FD mesh network is used to discretize the computational domains. A sample of such networking is shown in Fig.3. The governing differential equations (Eq. (6), Eq. (9) and Eq. (10)) are then replaced by their equivalent difference equations with truncation error of $O\ (h^2)$. All three equations follow the symmetric five-point FDM stencil shown in Fig.3.

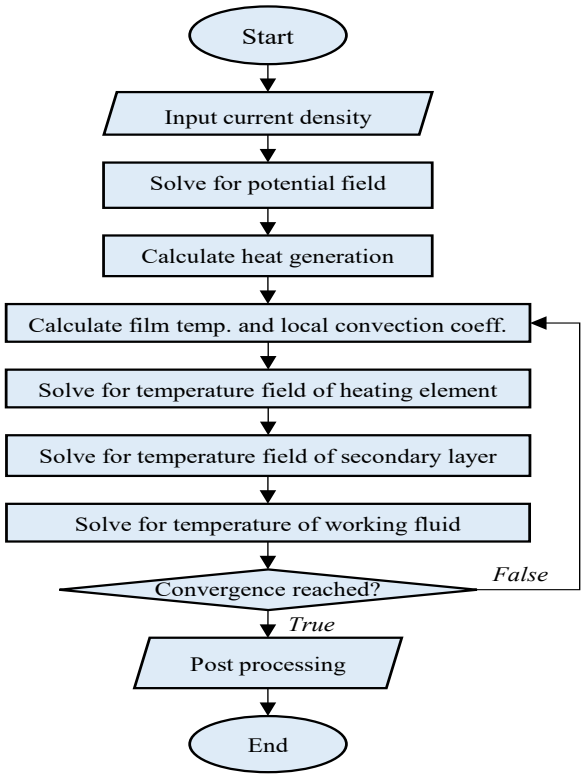


**Fig.4** Flow chart of the coupled analysis

The thermal problem consists of multiple interdependent domains. An efficient iterative scheme is developed to combine the correlated thermal problems – Eq. (9), Eq. (10) and Eq. (11) as well as couple them with the electrical problem. The flow diagram of the iterative scheme is presented in Fig.4.

## 6. Results and discussion

The electrothermal response of the *W-C(t)* electrical heating element is illustrated in Fig.5. The results are the potential field and three different temperature fields presented in the form of images. These results are obtained for an input current of $J = 1\text{x}10^7$ A/m$^2$ (40A) and an airflow of 10 m/s at a temperature of 300K. Similar images were found for *W-C(l)* and *Nichrome* with different field value ranges under identical test conditions.

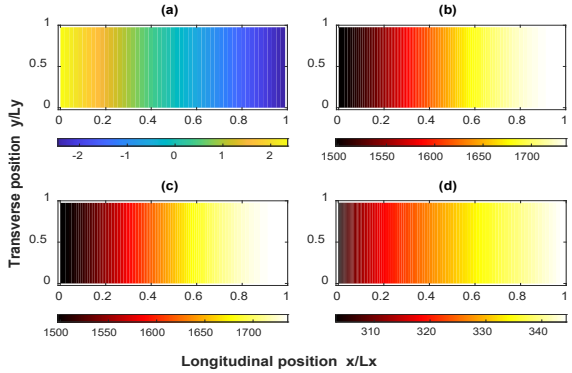


**Fig.5** Electrothermal response of *W-C(t)* of fiber volume fraction 0.4 under a dc field ($J = 1\text{x}10^7$ A/m$^2$): Image of (a) Potential field of the electrical heating element, (b) Temperature field of the electrical heating element, (c) Temperature field of the secondary layer and (d) Temperature distribution of air.

Fig.6 shows the comparison of electrothermal responses among *W-C(l)*, *W-C(t)* and *Ni-Cr* under a dc field of $J = 1\text{x}10^7$ A/m$^2$ (40A) and an airflow of 10 m/s at a temperature of 300K with both the composites having a fiber volume fraction of 0.4. The figure shows that the maximum potential difference is required for *W-C(t)*. As a result, a very high amount of heat is generated in the case of *W-C(t)* compared to others, which is reflected by the rise in temperature of the electrical heating element and the secondary layer. The rise in air temperature is remarkable in favor of *W-C(t)*.

Fig.7 shows composites and *Nichrome's* maximum resistive heating capacity before failure due to melting occurs. According to the figure, a maximum rise in air temperature of about 68K can be obtained in both orientations of the same fiber volume fraction composites at different current inputs.

The reason for getting the same temperature rise in both composite orientations is that the same failure criteria (melting point) were used in both cases. But the electrical resistivity changes along the direction of current flow; with that, the amount of heat generation varies with orientations under the same dc input. With significantly higher resistivity *W-C(t)* reaches the maximum temp rise at only $2\text{x}10^7$ A/m$^2$ (80A) input, while it takes *W-C(l)* almost $8\text{x}10^7$ A/m$^2$ (320A) input current to give the same output. *Nichrome* gives a 37K <

temperature rise for a similar input current to *W-C(t)* before failure.

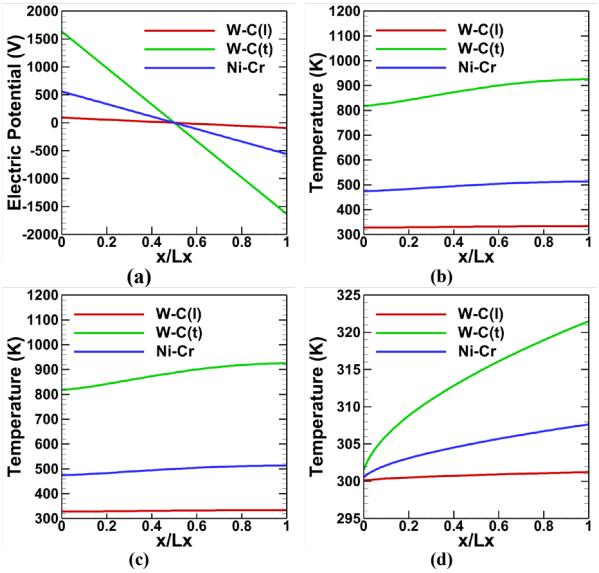


**Fig.6** Electro thermal response of *W-C(l)*, *W-C(t)* and Ni-Cr under a dc field ($J = 1x10^7$ A/m$^2$): the value of (a) Potential, (b) Temperature of the electrical heating element, (c) Temperature of the secondary layer and (d) Temperature of air, at the transverse position, $y/L_y = 0.5$

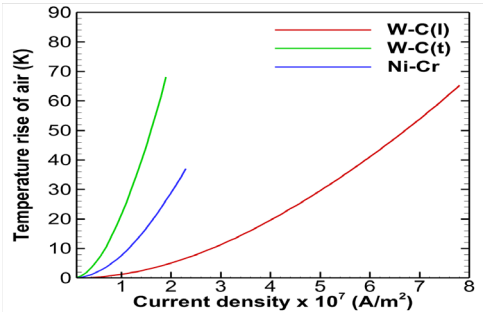


**Fig.7** Variation of Temperature rise of air at the exit of the resistive heating unit with current density

The resistive heating capability of the materials against input electric power is presented in Fig.8. This figure indicates that the efficiency of all three materials remains the same under a wide range of electrical inputs, which is represented by the slope of the curves that is almost equal to 1. Although *W-C(t)* requires less current than *W-C(l)* to provide a similar resistive heating effect, they both consume almost similar amounts of power input in terms of electric power.

The effect of different fiber volume fractions on resistive heating capacity is illustrated in Fig.9. The effect is analyzed under $J = 1x10^7$ A/m$^2$ (40A) and an airflow of 10 m/s at a temperature of 300K. As the output range is not the same for both orientations under the same input conditions, the temperature rises are illustrated by two separate y-axes. The resistive heating capability for both orientations rises with the increment of fiber content.

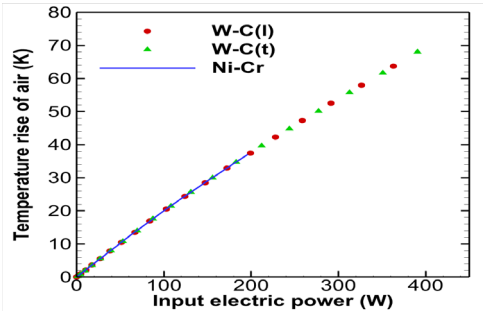


**Fig.8** Variation of Temperature rise of air at the exit of the resistive heating unit with input electric power

The rising trend of resistive heating capacity is more linear with the inclusion of fiber content in the *W-C(t)* case. On the other hand, *W-C(l)* shows a more parabolic trend.

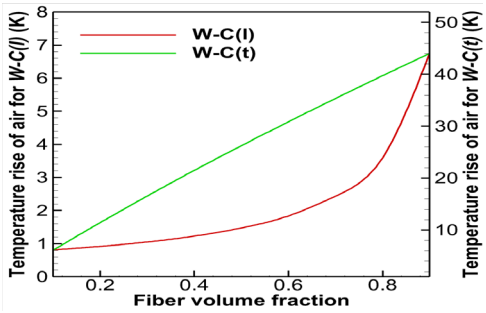


**Fig.9** Effect of change in fiber volume fraction of the composites in resistive heating applications under a dc flow of $J = 1x10^7$ A/m$^2$ (40A)

The accuracy of the present Finite Difference Method results is tested using the same materials and conditions, with a dc flow of $J = 1.5x10^7$ A/m$^2$ and average convection from the top face. The quantitative comparison shown in Table 2 illustrates that the results are in excellent agreement with those of commercial FEM solvers, confirming the scheme's appropriateness.

**Table 2** Comparison of the accuracy of results

| Material | Max Potential (mV) | | Max Temperature (K) | |
|---|---|---|---|---|
| | FDM | FEM | FDM | FEM |
| *W-C(l)* | 138.73 | 138.71 | 316.63 | 316.64 |
| *W-C(t)* | 2450.33 | 2450.42 | 594.02 | 594.05 |
| *Ni-Cr* | 840.04 | 840.00 | 400.79 | 400.80 |

## 7. Conclusions

The electrothermal behavior of *W-C(l)*, *W-C(t)* and *Nichrome* under the same conditions shows that *W-C(t)* exhibits better resistive heating performance than others. *W-C(t)* gives a 7% and 4.5% higher temperature rise of air than *W-C(l)* and traditional resistive heating elements *Nichrome,* respectively. However, with a very high input

current, *W-C(l)* can match the resistive heating capacity of *W-C(t)*. In this case, composites in both directions give air temperature rise up to 68K in contrast to a 37K rise by *Nichrome* before failure. The electrical heating efficiency of all three materials remains the same for a wide range of input electric power, implying that resistive heating is 100% energy efficient as almost all the incoming electric energy is converted into heat. The requirement of extra current for *W-C(l)* to match the resistive heating performance of *W-C(t)* indicates the requirement of higher electric potential in the case of *W-C(t)*. So, a similar rise in air temperature can be obtained at high voltage low current and low voltage high current conditions by simply applying current along transverse and longitudinal directions of the same composite element.

The resistive heating capacity of the composites increases significantly with the inclusion of fiber content. The trend is somewhat linear in the case of transverse orientation, whereas an exponential increment is noticed in the longitudinal orientation.

In the case of long-term resistive heating applications, low voltage and high current conditions should be discouraged. The major disadvantage of this heating condition is that it significantly affects the heating element's longevity. Exposure to high current density for longer intervals induces powerful electron wind that eventually causes failures due to electromigration by creating voids and hillocks along the heating element.

## 8. References


[1] J.-s. Lee, H. Jo, H.-s. Choe, Dae-sungLee, J. Hojin, L. Hye-ree, K. Jin-hwe, L. Hakjin, S. M. Rho and Y. Nam, "Electrothermal heating element with a nickel-plated carbon fabric for the leading edge of a wing-shaped composite application," *Composite Structures,* vol. 289, 2022.

[2] T.Aravind, S.Boominathasellarajan and N.Arunachalam, "Fabrication of Micro-channels on Polymethyl Methacrylate (PMMA) Plates by Thermal Softening Process Using Nichrome Wire: Tool Design and Surface Property Evaluation," *Procedia Manufacturing,* vol. 53, pp. 182-188, 2021.

[3] "KANTHAL," KANTHAL, [Online]. Available: https://www.kanthal.com/en/products/material-datasheets. [Accessed 2022].

[4] Y. HanKim, T. HoShin and Jae-haMyung, "MoSi2-based cylindrical susceptor for rapid high-temperature induction heating in air," *Ceramics International,* vol. 46, no. 15, pp. 23636-23642, 2020.

[5] H. Rujie, F. Daining, W. Peng, Z. Xinghong and Z. Rubing, "Electrical properties of ZrB2–SiC ceramics with potential for heating element applications," *Ceramics International,* vol. 40, no. 7, pp. 9549-9553, 2014.

[6] S. Priyaranjan, R. Pandu, M. Arabinda and M. Manas, "Recent progress in aluminum metal matrix composites: A review on processing, mechanical and wear properties," *Journal of Manufacturing Processes,* vol. 59, pp. 131-152, 2020.

[7] R. K.Sunil Kumar, M.Kannan, R.Karthikeyan, S. Althati and P.K.Jain, "Investigation of thermal and mechanical properties of Al7020/SiC/graphite hybrid metal matrix composites," *Materials Today Proceedings,* vol. 26, pp. 2746-2753, 2020.

[8] A.-C. Edwin, G. Sepideh and A. Leo, "Semi in-situ observation of crack initiation in compacted graphite iron during thermo mechanical fatigue," *International Journal of Fatigue,* vol. 137, 2020.

[9] W. Yujin, W. Dong and Z. Taiquan, "Refractory carbide reinforced tungsten matrix composites," *Journal of Alloys and Compounds,* vol. 925, 2022.

[10] D. L. Mc Danels, Electrical Resistivity And Conductivity Of Tungsten-Fiber-Reinforced Copper Composites, 1966.

[11] E. J. Barbero, Introduction to Composite Materials Design, 2017.

[12] B. Mutnuri, Thermal Conductivity Characterization of Composite Materials, Morgantown, West Virginia, 2006.

[13] O. A. Safer, S. Bensaid, D. Trichet and G. Wasselynck, "Transverse Electrical Resistivity Evaluation of Rod Unidirectional Carbon Fiber-Reinforced Composite Using Eddy Current Method," *IEEE Transactions on Magnetics,* vol. 54, pp. 1-4, 2018.

[14] A. Temesgen, Y. Qun and Z. Hui, "Conducting polymer-based thermoelectric composites: Principles, processing, and applications," in *Hybrid Polymer Composite Materials*, 2017, pp. 169-195.


## NOMENCLATURE

| | |
|---|---|
| $\varphi$ | : Electric potential, V |
| $G$ | : Joule heat generation, $W \cdot m^{-3}$ |
| $h$ | : Local convection coefficient, $W \cdot m^{-2} \cdot K^{-1}$ |
| $J$ | : Input current density, $A \cdot m^{-2}$ |
| $k_l, k_t$ | : Longitudinal & transverse thermal conductivity of composite, $W \cdot m^{-1} \cdot K^{-1}$ |
| $k_m$ | : Thermal conductivity of matrix, $W \cdot m^{-1} \cdot K^{-1}$ |
| $k_f$ | : Thermal conductivity of fiber, $W \cdot m^{-1} \cdot K^{-1}$ |
| $L_x, L_y$ | : Length and Width of heating plate, mm |
| *Ni-Cr* | : *Nichrome (Ni 80%- Cr 20%)* |
| $\rho_l, \rho_t$ | : Longitudinal & transverse electrical resistivity of composite, Ω m |
| $\rho_m, \rho_f$ | : Electrical resistivity of matrix & fiber, Ω m |
| $t$ | : Thickness of heating plate, μ m |
| $T_1, T_2, T_a$ | : Temperature, K |
| $V_m, V_f$ | : Volume fraction of matrix & fiber |
| *W-C(l)* | : Composite of longitudinal fiber orientation. |
| *W-C(t)* | : Composite of transverse fiber orientation. |